Combined Subband-Subcarrier Spectral Shaping in Multi-Carrier Modulation under the Excess Frame Length Constraint

Dong-Jun Han, *Student Member, IEEE,* Jaekyun Moon, *Fellow, IEEE,* Dongjae Kim, *Student Member, IEEE,* Sae-Young Chung, *Senior Member, IEEE,* and Yong H. Lee, *Senior Member, IEEE*

Abstract—This paper investigates spectral shaping of multi-carrier-modulation (MCM) waveforms based on combination of Nyquist windowing and subband filtering. The combined windowing/filtering allows simultaneous control on both subcarrier and subband spectra. When compared to existing Nyquist windowing or subband filtering techniques under a fixed excess frame length constraint, the proposed scheme offers reduced sensitivity to carrier frequency and symbol timing offsets. Establishing an analytical tool based on the error spectrum stack consisting of the error signals evaluated at different signal delay positions, we explore the window-filter trade-off and provide the minimum interference power solution for given ranges of carrier frequency and symbol timing offsets. Our design targets low-latency applications having no provisions for high-precision synchronization and having potential need for spectrum aggregation.

Index Terms—Waveform design, low latency, tactile communication, OFDM, universal filtered multi-carrier (UFMC), carrier-frequency offset (CFO), symbol-timing offset (STO)

I. INTRODUCTION

IN air-interface design of future tactile communication [1], minimizing transmission-reception latency is of paramount importance. Views already exists that advocate a one-way end-to-end physical-layer latency as low as 100 μs in achieving a round-trip communication delay of 1 ms or so, a value considered necessary in the context of tactile communication [2], [3]. Under such a tight latency constraint, precise closed-loop synchronization becomes increasingly challenging. This is especially true in the Internet of Things (IoT) environment where a massive number of low-cost devices coexist in the network. The high-precision synchronization requirement is costly in terms of both latency and implementation complexity; spectral efficiency may also need to be compromised due to a substantial amount of preamble data necessary. Efforts are already under way as part of 5G planning to make provisions for a special type of traffic for sporadic sensor/actor messages requiring low latencies, e.g., type III traffic in [4].

Another critical requirement of future communication standards related to the IoT is to maintain low signal radiation into neighboring frequency bands. This need arises when spectrum aggregation is exercised in an effort to accommodate a large number of users and/or deliver a maximum total data throughput given highly fragmented frequency spectra of the heterogeneous IoT environment. Without tight spectral leakage control, one user's signal quality in a given frequency band is seriously affected by the presence of another users in nearby spectral bands.

The current multi-carrier communication standards based on traditional orthogonal-frequency-division-multiplexing (OFDM) may be able to support the sub-millisecond overall communication latency requirement by simply adopting a short frame time (and a larger number of subcarriers in meeting the required data size). However, OFDM is notoriously sensitive to the carrier-frequency offsets (CFOs) and symbol timing offsets (STOs)[1] that will be increasingly severe in the future IoT environment with numerous commodity devices lacking sophisticated synchronization mechanism. This major shortcoming of the current OFDM technology is largely due to the broad main lobe as well as the slowly-decaying sidelobes of the subcarrier spectra, which also lead to a substantial amount of signal leakage into neighboring bands and thus problematic interferences.

In this paper, we investigate ways of improving OFDM, specifically focusing on combining filtering with Nyquist windowing to counter the effect of CFO/STOs. We also provide a minimum out-of-band power (OBP) leakage solution. We look at this issue under a tight excessive time frame length constraint with the goal in mind to maximize the time-efficiency and minimize the transmission/reception delay.

There have been a number of approaches proposed to improve MC modulation via spectral shaping. Various Nyquist windowing techniques that retain the orthogonal property of the subcarriers have been studied extensively, mainly to reduce inter-carrier interference induced by the CFO [5]–[8]. Of the more recently advocated approaches on spectral control is the filter-bank multicarrier (FBMC) [9], [10]. FBMC creates waveforms that are highly robust to asynchronicity, but the resulting time-domain pulse is rather long, making the scheme unsuitable for low-latency applications. Generalized frequency division multiplexing (GFDM) is a technique that provides flexibility to existing OFDM by allowing multiple time symbols per subcarrier [11], [12], giving a considerable savings in terms of time overhead allocated to cyclic prefix. Through cyclic-filtering, GFDM also provides some amount of spec-

[1]assuming a small cyclic prefix (CP) overhead, which is a trend.

trum shaping but extra windowing and/or spectral guard bands are typically needed to provide adequate OBP suppression [12]. The complexity and latency associated with near-optimal detection needed to undo self-interferences within a frame are also a concern for GFDM. Finally, others have argued for spectral shaping by subband of subcarriers through filtering [13]. This technique, referred to as universal filtered multi-carrier (UFMC), requires time-domain convolution of digital filters with time-converted data symbols in each subband. As such, complexity is higher than simple time-windowing and the time-domain convolution gives rise to a time leak of the signal, resulting in an excess frame length relative to the CP-less OFDM data frame. The advantage is that substantial OBP reduction is achieved leading to improved robustness against CFO and STO. In fact, there already have been attempts to design filters to maximize certain metrics related to subcarrier signal-to-interference ratios (SIRs), when the interferences arise due to CFO/STO [14], [15].

In this paper, we also consider subband filtering for MCM. However, unlike in previous studies on the subject, we investigate ways to optimally combine filtering with Nyquist windowing under a fixed excess frame length constraint. Our contributions are as follows. We establish an analytical tool that provides considerable insights into the impact of window/filter on interference mitigation and allows convenient window/filter design optimization. The feature of our analysis starts from a view point that subband filtering at the transmitter is to impose various delays in the transmission time of the signal. We introduce the notion of the error spectrum stacking, which collects the CFO/STO-induced error signal spectra evaluated at different signal delay positions. Given a fixed excess frame length constraint, the error spectrum stack depends on the Nyquist window only, not on the filter. The filtering effect comes into play as the tap weights provide different weights on the stacked error signals. The window-filter trade-off is investigated by looking at the optimal window/filter length combination. Throughout the paper we make use of an efficient receiver structure based on "tail-biting" followed by the usual N-point DFT, rather than the $2N$-point DFT employed in previous works targeting either window or filter [14]–[16]. Based on our analytical tool, we explore trade-off between windowing and filtering and show that given a fixed excess frame length a judicious combination of windowing and filtering offers improved spectral control and thus better performance in CFO/STO. We also provide a minimum out-of-band power solution.

The following symbols and notations are used throughout. A vector $\mathbf{x}$ is a row vector, which allows easier visualization of sequential sample processing. A capitalized bold letter $\mathbf{X}$ means either a row vector representing the frequency-domain samples or a matrix; the distinction will be made clear whenever needed. The symbol $\circ$ denotes the entry-wise (Hadamard) product. The symbol $\mathbf{x}_a^b$ represents a row-vector segment of elements $[x_a\ x_{a+1}\cdots x_b]$ for $a < b$ or $[x_a\ x_{a-1}\cdots x_b]$ for $a > b$. The superscript " $\to k$" in $\mathbf{x}^{\to k}$ is to denote a right cyclic-shift of $\mathbf{x}$ by k positions (with a negative k meaning a left cyclic-shift). The symbol $\circledast$ denotes the circular convolution. The symbol $\mathbf{1}_j$ means a row vector segment of j
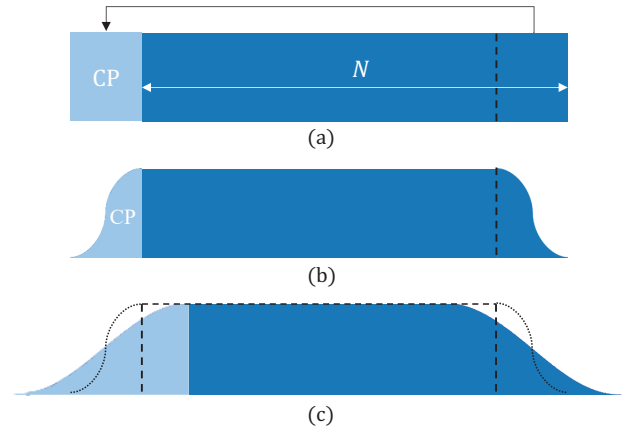

Fig. 1. Single-data-symbol packet transmission with combined Nyquist-windowing and filtering; (a) After adding CP, (b) after Nyquist windowing, and (c) after side-band filtering.

consecutive 1s while $\mathbf{0}_j$ represents a similarly defined string of 0s. A related symbol $\mathbf{1}$ corresponds to a vector full of 1s. $\mathbf{X}_*$, $\mathbf{X}^H$ denote conjugate and conjugate transpose of matrix $\mathbf{X}$ respectively. An overbar denotes statistical expectation.

II. Signal Transmission and Reception

We consider a single-data-symbol packet transmission for tactile communication where minimizing end-to-end communication latency is the most critical factor while the total amount of transmitted data is relatively small. See [17] for latest proposal for single-symbol transmission. The frame structure for our proposed combined windowing and filtering is seen in Fig. 1. A cyclic prefix of a given length is first created and then a window is applied whose transition width completely covers the entire CP as well as the tail data that generated the CP. This windowing is further followed by subband-by-subband filtering as done in UFMC, which further broadens the received data frame. N_{ex} denotes the excess length beyond the original symbol frame length of N.

Let $\mathbf{S}(i) = [S_0(i)\ S_1(i)\ \cdots\ S_{N_{sb}-1}(i)]$ be the row vector of the frequency-domain data symbols for subband i consisting of N_{sb} contiguous subcarriers. Let $\mathbf{X}(i)$ be the N-element row vector including $\mathbf{S}(i)$ as its i-th segment with padded zeros elsewhere: $\mathbf{X}(i) = [\mathbf{0}_{(i-1)N_{sb}}\ \mathbf{S}(i)\ \mathbf{0}_{N-iN_{sb}}]$ where $\mathbf{0}_l$ denotes a string of l zeros. Let $\mathbf{x}(i)$ be the inverse DFT of $\mathbf{X}(i)$ that spread to N time samples. Let $\mathbf{y}(i)$ be the signal vector obtained after prefixing the last N_{cp} samples of $\mathbf{x}(i)$ and applying the Nyquist window, i.e.,

$$\mathbf{y}(i) = [\mathbf{x}(i)_{N-N_{cp}}^{N-1}\circ\mathbf{w}_1^{N_{cp}}\quad \mathbf{x}(i)_0^{N-N_{cp}-1}\quad \mathbf{x}(i)_{N-N_{cp}}^{N-1}\circ\mathbf{w}_{N_{cp}}^1]$$

where the window transition shape determined by $\mathbf{w}_1^{N_{cp}} = [w_1\ w_2\ \cdots\ w_{N_{cp}}]$ is symmetric between the left and right edges with the coefficients w_j's taking values between 0 and 1.

Let $g_k(i) = g_k e^{j2\pi\Omega_i k}$, $0 \le k \le L_g - 1$, be the transmitter filter impulse response samples for subband i with center frequency Ω_i and length L_g, which is assumed to be the

same for all i. In general each subband may experience a different channel (e.g., in uplink where multiple users from different locations send data on different subbands). Letting $h_k(i)$, $0 \leq k \leq L_h - 1$, be the channel impulse response samples for subband user i, think of a combined filter/channel response $v_k(i) = (h(i) * g(i))_k$ for subband i. The filtered data for subband i is now

$$z_k(i) = \sum_{l=0}^{L_v - 1} y_{k-l}(i) v_l(i)$$

where $y_j(i)$ are components of $\mathbf{y}(i)$ and $L_v = L_g + L_h - 1$ is the combined subband filter and channel response length with L_h denoting the maximum channel delay spread regardless of i. Summing up all signals transmitted from all subbands, we get the received signal samples

$$r_k = \sum_{i \in C_{sub}} z_k(i) + n_k$$

where C_{sub} is the set of all subband indices and n_k is random noise.

Collect the received time-domain signal samples in an extended row vector:

$$\mathbf{r} = [r_0 \ r_1 \ r_2 \ \cdots \ r_{N-1} \ r_N \ \cdots \ r_{N+N_t-1}]$$

where N_t represents the number of additional tail samples beyond N, the DFT frame length. We set $N_t = N_{cp} + L_v - 1$, which is the minimum tail length needed to have a chance to recover all transmitted symbols, as will be clear soon. Express the "tail-biting" operation of taking the last N_t samples of $\mathbf{r}$ and adding them to the first N_t samples pairwise as $\mathbf{r\Gamma}$, where

$$\mathbf{\Gamma} = \begin{bmatrix} \mathbf{I}_N \\ \hline \mathbf{I}_{N_t} \ \ \mathbf{0} \end{bmatrix}$$

with $\mathbf{I}_m$ denoting the identity matrix with dimension m and $\mathbf{0}$ an all-zero matrix filling the gap (with dimension N_t by $N - N_t$).

It can be shown that taking an N-point DFT of $\mathbf{r\Gamma}$ recovers the transmitted frequency-domain symbols for all subbands under some particular condition on the window shape and assuming that the filter/channel responses are known. We state this formally in a lemma below. Let $\mathbf{F}$ be the DFT matrix with column k, $0 \leq k \leq N - 1$, specified as $[1 \ e^{-j2\pi k/N} \ \cdots \ e^{-j2\pi(N-1)k/N}]^T$. Let $\mathbf{V}(i) = [V_0(i) \ \ V_1(i) \ \ \cdots \ \ V_{N-1}(i)]$ be the DFT of the zero-padded version of the combined filter/channel impulse response $\mathbf{v}(i) = [v_0(i) \ v_1(i) \ \cdots \ v_{L_v-1}(i) \ \mathbf{0}_{N-L_v}]$. The vector $\mathbf{\bar{r}\Gamma F}$ represents a tail-biting/DFT operation on $\mathbf{\bar{r}}$, the noiseless portion of $\mathbf{r}$. Think of this vector as made up of $N_u = N/N_{sb}$ non-overlapping contiguous segments. We have the following property (with proof given in Appendix A).

Lemma 1. The vector $\mathbf{\bar{r}\Gamma F}$ collects the original data symbols, $\mathbf{S}(0), \mathbf{S}(1), \cdots, \mathbf{S}(N_u - 1)$, weighted by the combined filter/channel transfer function samples with a known phase-

rotation in the following sense:

$$\mathbf{\bar{r}\Gamma F}$$
$$= \mathbf{P}(N_{cp}) \circ [\mathbf{V}(0)_0^{N_{sb}-1} \circ \mathbf{S}(0) \quad \mathbf{V}(1)_{N_{sb}}^{2N_{sb}-1} \circ \mathbf{S}(1)$$
$$\cdots \ \mathbf{V}(N_u - 1)_{N-N_{sb}}^{N-1} \circ \mathbf{S}(N_u - 1)] \quad (1)$$

if $\mathbf{w}_1^{N_{cp}} + \mathbf{w}_{N_{cp}}^1 = \mathbf{1}$, where $\mathbf{1}$ denotes a vector of all 1s, and $\mathbf{P}(k) = [1 \ e^{-j2\pi k/N} \ \cdots \ e^{-j2\pi(N-1)k/N}]$ is a phase-rotation vector.

The above window shaping condition $\mathbf{w}_1^{N_{cp}} + \mathbf{w}_{N_{cp}}^1 = \mathbf{1}$ implies that given the symmetry condition between $\mathbf{w}_1^{N_{cp}}$ and $\mathbf{w}_{N_{cp}}^1$, the coefficients must be odd-symmetric around its mid-point, i.e., $w_{j+1} = 1 - w_{N_{cp}-j}$ for all $0 \leq j \leq N_{cp} - 1$, the classical Nyquist pulse-shaping condition giving rise to zero ICI among subcarriers.

III. FILTER AND WINDOW DESIGN

The ideal symbol recovery at the receiver guaranteed by Lemma 1 applies only to perfect time and frequency synchronization. Assuming a MC-symbol timing offset and/or a carrier frequency offset, however, the choice of the window and the filter makes difference. What is the best window length and filter combination for our purposes?

In this work, we focus on the window shape that gives rise to the raised-cosine family of subcarrier spectra. Thus, the window shape and length are controlled by a single parameter $\beta = N_{cp}/N$. Recall that N_{ex} denotes the excess frame length. The first design choice is to decide what portion of N_{ex} should be allocated to windowing. Let α represent the portion of N_{ex} allocated to windowing, i.e., $\alpha = \beta N/N_{ex}$. Then the filter length would be $L_g = N_{ex} - \beta N + 1 = (1 - \alpha)N_{ex} + 1$. For given β, choosing $\alpha = 0$ reduces the system to UFMC while taking $\alpha = 1$ implies pure Nyquist windowing with a complete bypassing of the subband filtering. What is the best filter shape for a given window size? In the end we are interested in finding the best combination of N_{cp} and the filter response $\mathbf{g}$. Considering other kinds of window shapes or extending the work to a joint optimization of window function, filter, N_{cp} is an interesting topic for future research.

A. CFO/STO-Induced Error Signal

While it is more reasonable and realistic to assume the presence of both STO and CFO, treating each individually as a sole source of interference provides a more clear and intuitive picture. Analysis on combined STO and CFO effect will be carried out after the interference analysis on individual effects.

It is helpful again to just focus on $\mathbf{y}(i)$ arriving in the l-th multi-path, one particular component of $\mathbf{z}(i)$. To reduce notational cluttering, we suppress the subband index i for the time being, unless clarity is required. Consider an STO of τ, ignoring CFO momentarily. The signal arriving in the l-th path captured in a shifted DFT-plus-tail frame due to an STO of τ samples, $\mathbf{y}_\tau(l)$, actually experiences an effective STO of $l - \tau$. This can be seen in Fig. 2.
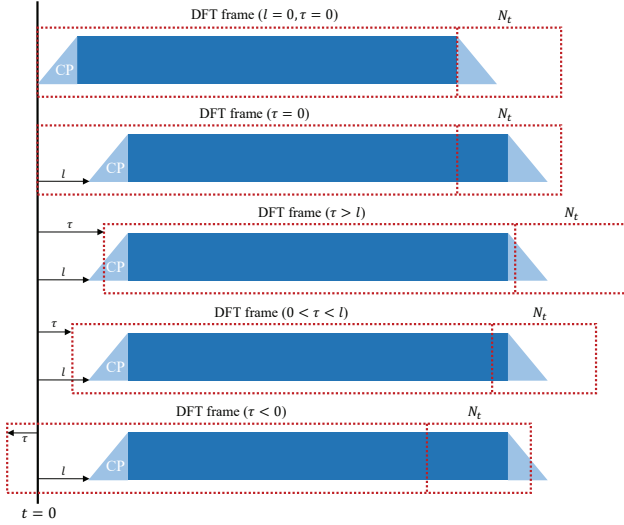
Fig. 2. Captured data frames for different values of l and τ.

The captured data, after tail-biting, can be expressed as

$$\mathbf{y}_\tau(l)\mathbf{\Gamma} = \mathbf{x}^{\rightarrow(l-\tau+N_{cp})} \circ \mathbf{d}_\tau(l) \tag{2}$$

where $\mathbf{d}_\tau(l)$ represents a data capture frame due to an effective timing offset of $l - \tau$. At certain positions within the capture frame, the data samples may get distorted by the misaligned left and right window edges. At certain other positions data may simply get lost completely. Visual inspection of the capture frames in Fig. 2 for different values of $\rho \triangleq l - \tau$ given N_{cp} and N_t leads to the following characterization:

$$\mathbf{d}_\tau(l) = \begin{cases} [\mathbf{1}_{N_t} \ \mathbf{0}_{\rho-N_t} \ \mathbf{w}_1^{N_{cp}} \ \mathbf{1}_{N-N_{cp}-\rho}], \\ \qquad\qquad N_t + 1 \le \rho \le N - N_{cp} - 1 \\ [\mathbf{1}_{N_t} \ \mathbf{w}_{1+N_t-\rho}^{N_{cp}} \ \mathbf{1}_{N-N_{cp}-\rho}], \\ \qquad\qquad N_t - N_{cp} + 1 \le \rho \le N_t \\ [\mathbf{1}_N], \qquad\qquad 0 \le \rho \le N_t - N_{cp} \\ [\mathbf{1}_{N-|\rho|} \ \mathbf{w}_{N_{cp}}^{N_{cp}-|\rho|+1}], \quad -(N_{cp}-1) \le \rho \le -1 \\ [\mathbf{1}_{N-|\rho|} \ \mathbf{w}_{N_{cp}}^1 \ \mathbf{0}_{|\rho|-N_{cp}}], \qquad -N_t \le \rho \le -N_{cp} \end{cases} \tag{3}$$

where $\mathbf{1}_j$ is a string of j consecutive 1s. The captured data sample positions occupied by 1 mean no distortion, whereas those given by window coefficients signify loss of signal amplitude. The positions of 0s indicate a complete drop of the data samples due to a large misalignment between the actual received signal and the capture frame.

Let us now consider the effect of normalized CFO of c without any STO. The signal arriving in the l-th path can be written, after tail-biting, as

$$\mathbf{y}_c(l)\mathbf{\Gamma} = \mathbf{x}^{\rightarrow(l+N_{cp})} \circ \mathbf{d}_c(l) \circ \mathbf{q}_c \tag{4}$$

where

$$\mathbf{d}_c(l) = [e^{j2\pi c} \times \mathbf{1}_l \ (w_1 + w_{N_{cp}}e^{j2\pi c}) \ (w_2 + w_{N_{cp}-1}e^{j2\pi c}) \\ \cdots \ (w_{N_{cp}} + w_1 e^{j2\pi c}) \ \mathbf{1}_{N-N_{cp}-l}], \tag{5}$$

and

$$\mathbf{q}_c = [1 \quad e^{j2\pi c/N} \quad e^{j2\pi c(2)/N} \quad \cdots \quad e^{j2\pi c(N-1)/N}]. \tag{6}$$

The vector $\mathbf{q}_c$ introduces CFO whereas the Nyquist window function $\mathbf{w}$ enfolded in the data capture frame vector $\mathbf{d}_c(l)$ plays a role of countering the ICI caused by $\mathbf{q}_c$.

Under both STO and CFO, the captured signal arriving in the l-th path upon tail-biting is written as

$$\mathbf{y}_{\tau,c}(l)\mathbf{\Gamma} = \mathbf{x}^{\rightarrow(l-\tau+N_{cp})} \circ \mathbf{d}(l) \circ \mathbf{q} \tag{7}$$

where subband index i is again suppressed, $\mathbf{d}(l)$ is a data capture frame now due to both τ and c and

$$\mathbf{q} = e^{j2\pi\tau c/N}[1 \quad e^{j2\pi c/N} \quad e^{j2\pi c(2)/N} \quad \cdots \quad e^{j2\pi c(N-1)/N}].$$

With both CFO and STO, straightforward visual inspection, albeit tedious, leads to

$$\mathbf{d}(l) = \begin{cases} [e^{j2\pi c} \times \mathbf{1}_{N_t} \ \mathbf{0}_{\rho-N_t} \ \mathbf{w}_1^{N_{cp}} \ \mathbf{1}_{N-N_{cp}-\rho}], \\ \qquad\qquad N_t + 1 \le \rho \le N - N_{cp} - 1 \\ [e^{j2\pi c} \times \mathbf{1}_\rho \ (\mathbf{w}_1^{N_t-\rho} + \mathbf{w}_{N_{cp}}^{N_{cp}-N_t+\rho+1}e^{j2\pi c}) \\ \qquad \mathbf{w}_{1+N_t-\rho}^{N_{cp}} \ \mathbf{1}_{N-N_{cp}-\rho}], \\ \qquad\qquad N_t - N_{cp} + 1 \le \rho \le N_t \\ [e^{j2\pi c} \times \mathbf{1}_\rho \ \mathbf{w}_1^{N_{CP}} + \mathbf{w}_{N_{CP}}^1 e^{j2\pi c} \ \mathbf{1}_{N-N_{CP}-\rho}], \\ \qquad\qquad 0 \le \rho \le N_t - N_{cp} \\ [(\mathbf{w}_{|\rho|+1}^{N_{cp}} + \mathbf{w}_{N_{cp}-|\rho|}^1 e^{j2\pi c}) \ \mathbf{1}_{N-N_{cp}} \ \mathbf{w}_{N_{cp}}^{N_{cp}-|\rho|+1}], \\ \qquad\qquad -(N_{cp}-1) \le \rho \le -1 \\ [\mathbf{1}_{N-|\rho|} \ \mathbf{w}_{N_{cp}}^1 \ \mathbf{0}_{|\rho|-N_{cp}}], \quad -N_t \le \rho \le -N_{cp} \end{cases} \tag{8}$$

where $\rho = l - \tau$.

The total power of the interference due to an STO of τ and a CFO of c arising in subband i (and spilling into other subbands) depends on both the Nyquist window $\mathbf{w}$ and the combined filter/channel $\mathbf{v}$. To focus on the role of the transmit filter $\mathbf{g}$ in countering the effect of CFO/STO, however, we assume in the sequel that the channel is ideal, i.e., $\mathbf{v} = \mathbf{g}$.

Without losing generality focus on the subband centered at DC and assume that the first frequency bin corresponds to DC. Although not critical, we will also assume in the sequel that there are an odd number of subcarriers within a subband to maintain symmetry around DC. Let $N_{sb} = 2N_1 + 1$ for some integer N_1. The captured l-th multipath signal (caused by subband filtering) after tail-biting can be written in the frequency domain as

$$\mathbf{y}_{\tau,c}(l)\mathbf{\Gamma}\mathbf{F} = [\mathbf{X} \circ \mathbf{P}(l - \tau + N_{cp})] \circledast \mathbf{A}(l) \tag{9}$$

where $\circledast$ denotes circular convolution of two row vectors and $\mathbf{A}(l)$ is the DFT of $\mathbf{d}(l) \circ \mathbf{q}$. This N-dimensional vector spreads across N frequency bins in general. For the signals within the subband of interest, we assume that the common phase rotation component τ can be compensated. So the captured signal after tail-biting can be written as

$$\mathbf{y}_{\tau,c}(l)\mathbf{\Gamma}\mathbf{F} = [\mathbf{X} \circ \mathbf{P}(l - \tau + N_{cp}) \circledast \mathbf{A}(l)] \circ \mathbf{P}(\tau) \tag{10}$$
$$= \mathbf{X}\mathbf{P}_{l-\tau+N_{cp}}\mathbf{A}_l\mathbf{P}_\tau. \tag{11}$$

where the vector-matrix representation is introduced in the second line to reduce notational cluttering, with $\mathbf{P}_j$ denoting

a diagonal matrix taking elements from the vector $\mathbf{P}(j)$ and $\mathbf{A}_l$ being a circular convolution matrix for whose n-th row corresponds to the n-th cyclic shift of $\mathbf{A}(l)$.

B. Error Calculations

Within the subband of interest, the error signal is then $[\mathbf{y}(l) - \mathbf{y}_{\tau,c}(l)]\mathbf{\Gamma F}$. Defining a mask matrix that suppresses all signals leaking outside the given subband

$$\mathbf{M}_{ib} = \text{diag}[\underbrace{1\ 1\ \cdots\ 1}_{1+N_1}\ 0\ 0\cdots 0\ 0\ \underbrace{1\ \cdots\ 1}_{N_1}],$$

and summing up the captured l-th multipath signal according to the filter weights g_l, we can write the frequency-domain in-band-only error as

$$\mathbf{e}_{ib} \triangleq \sum_{l=0}^{L_g-1} g_l[\mathbf{A}(l)_0\mathbf{y}(l) - \mathbf{y}_{\tau,c}(l)]\mathbf{\Gamma F M}_{ib} \qquad (12)$$

$$= \sum_{l=0}^{L_g-1} g_l[\mathbf{A}(l)_0\mathbf{X P}_{l+N_{cp}} - \mathbf{X P}_{l-\tau+N_{cp}}\mathbf{A}_l\mathbf{P}_\tau]\mathbf{M}_{ib}$$

$$= \sum_{l=0}^{L_g-1} g_l\mathbf{X P}_{l+N_{cp}}[\mathbf{A}(l)_0\mathbf{I} - \mathbf{P}_{-\tau}\mathbf{A}_l\mathbf{P}_\tau]\mathbf{M}_{ib}$$

$$= \sum_{l=0}^{L_g-1} g_l\boldsymbol{\epsilon}_{ib}(l)\mathbf{M}_{ib} \qquad (13)$$

where $\mathbf{A}(l)_0$ is the 0-th element of $\mathbf{A}(l)$ and

$$\boldsymbol{\epsilon}_{ib}(l) \triangleq \mathbf{X P}_{l+N_{cp}}[\mathbf{A}(l)_0\mathbf{I} - \mathbf{P}_{-\tau}\mathbf{A}_l\mathbf{P}_\tau], \qquad (14)$$

which can be viewed as the l-specific error vector. By multiplying $\mathbf{A}(l)_0$ with each l-th multipath undistorted signal in equation (12), the original signal power becomes the same as the one with CFO/STO for each subcarrier. This makes the error vector to contain only the in-band distortion, not the signal difference.

$$\mathbf{e}_{ob} \triangleq \sum_{l=0}^{L_g-1} g_l\mathbf{y}_{\tau,c}(l)\mathbf{\Gamma F M}_{ob}$$

$$= \sum_{l=0}^{L_g-1} g_l\mathbf{X P}_{l-\tau+N_{cp}}\mathbf{A}_l\mathbf{M}_{ob}$$

$$= \sum_{l=0}^{L_g-1} g_l\boldsymbol{\epsilon}_{ob}(l)\mathbf{M}_{ob} \qquad (15)$$

where

$$\mathbf{M}_{ob} = \text{diag}[\underbrace{0\ 0\ \cdots\ 0}_{1+N_1}\ 1\ 1\cdots 1\ 1\ \underbrace{0\ \cdots\ 0}_{N_1}],$$

a similar mask that suppresses all signals inside the given subband, and

$$\boldsymbol{\epsilon}_{ob}(l) \triangleq \mathbf{X P}_{l-\tau+N_{cp}}\mathbf{A}_l. \qquad (16)$$

This vector $\mathbf{e}_{ob}$ is the error spectrum spread across the $N - N_{sb}$ frequency bins due to the interference leaking into other subbands. Note that for outside of the main subband, it is assumed that the phase rotaion τ is not compensated.

By stacking up the row vectors $\boldsymbol{\epsilon}_{ob}(0), \boldsymbol{\epsilon}_{ob}(1), \cdots, \boldsymbol{\epsilon}_{ob}(L_g-1)$ from top to bottom in matrix $\mathbf{E}_{ob}$ and, likewise for $\mathbf{E}_{ib}$, we can write

$$\mathbf{e}_{ob} = \mathbf{g E}_{ob}\mathbf{M}_{ob} \qquad (17)$$

$$\mathbf{e}_{ib} = \mathbf{g E}_{ib}\mathbf{M}_{ib}. \qquad (18)$$

The stacked error spectra $\mathbf{E}_{ob}$ and $\mathbf{E}_{ib}$ with row l corresponding to $\boldsymbol{\epsilon}_{ob}(l)$ and $\boldsymbol{\epsilon}_{ib}(l)$, respectively, are functions only of the Nyquist window; they do not depend on the filter. Let $\mathbf{\Lambda}_{ob} = \overline{\mathbf{E}_{ob}\mathbf{M}_{ob}\mathbf{M}_{ob}^H\mathbf{E}_{ob}^H}$, $\mathbf{\Lambda}_{ib} = \overline{\mathbf{E}_{ib}\mathbf{M}_{ib}\mathbf{M}_{ib}^H\mathbf{E}_{ib}^H}$. Then, the interference power for out-of-band and in-band generated by all subcarriers in a specific subband becomes

$$J_{ob} \triangleq \overline{||\mathbf{e}_{ob}||^2} = \mathbf{g}\overline{\mathbf{E}_{ob}\mathbf{M}_{ob}\mathbf{M}_{ob}^H\mathbf{E}_{ob}^H}\mathbf{g}^H = \mathbf{g}\mathbf{\Lambda}_{ob}\mathbf{g}^H \qquad (19)$$

$$J_{ib} \triangleq \overline{||\mathbf{e}_{ib}||^2} = \mathbf{g}\overline{\mathbf{E}_{ib}\mathbf{M}_{ib}\mathbf{M}_{ib}^H\mathbf{E}_{ib}^H}\mathbf{g}^H = \mathbf{g}\mathbf{\Lambda}_{ib}\mathbf{g}^H \qquad (20)$$

and we can define the total interference power as

$$J \triangleq J_{ob} + J_{ib} = \mathbf{g}(\mathbf{\Lambda}_{ob} + \mathbf{\Lambda}_{ib})\mathbf{g}^H = \mathbf{g}\mathbf{\Lambda}\mathbf{g}^H \qquad (21)$$

where $\mathbf{\Lambda} = \mathbf{\Lambda}_{ob} + \mathbf{\Lambda}_{ib}$. This total interference power J, is the power that we wish to reduce as much as possible.

On the other hand, we would like to enhance the signal power of the subband of interest, which has loss due to CFO/STO. From the n-th element of (11), and taking only the signal portion, the distorted signal of the n-th subcarrier has the weight of

$$\sum_{l=0}^{L_g-1} g_l[\mathbf{P}(l + N_{cp})_n\mathbf{A}(l)_0]. \qquad (22)$$

This can be rewritten as $\mathbf{g}\mathbf{u}^H(n)$ where $\mathbf{u}(n)$ is the row vector of length L_g with $\mathbf{P}^*(l + N_{cp})_n\mathbf{A}^*(l)_0$ as its l-th element. The power of the n-th signal can be written as $\mathbf{g}[\sigma_X^2\mathbf{u}^H(n)\mathbf{u}(n)]\mathbf{g}^H$, where $\sigma_X^2 = \overline{|X_n|^2}$. Considering the subband centered around the first subcarrier, we can define the total signal power of the subcarriers of interest as

$$Q \triangleq \mathbf{g}[\sigma_X^2\sum_{n=-N_1}^{N_1}\mathbf{u}^H(n)\mathbf{u}(n)]\mathbf{g}^H = \mathbf{g}\mathbf{\Psi}\mathbf{g}^H \qquad (23)$$

where $\mathbf{\Psi} \triangleq \sigma_X^2\sum_{n=-N_1}^{N_1}\mathbf{u}^H(n)\mathbf{u}(n)$. We utilized the cyclic property $\mathbf{P}(l)_{N+t} = \mathbf{P}(l)_t$ for the case $t < 0$.

C. Optimization of Signal to Interference Ratio

Now the optimization goal is to maximize the ratio Q/J for a given set $\{N_{ex}, \alpha\}$. Let $\lambda_{max}\{\mathbf{V}\}$ denote the maximum eigenvalue of $\mathbf{V}$ and $\phi_{max}\{\mathbf{V}\}$ the corresponding eigenvector of $\mathbf{V}$. The following lemma allows us to find the optimal filter tap weights, in the sense of maximizing Q/J, under a fixed excess frame length constraint and a given window size.

Lemma 2. The filter $\mathbf{g}$ of length $L_g = (1 - \alpha)N_{ex} + 1$ that maximizes the power ratio Q/J under the constraint $||\mathbf{g}||^2 = 1$ is given by

$$\mathbf{g}_{opt} = c\ \phi_{max}\{\mathbf{\Lambda}^{-1}\mathbf{\Psi}\} \qquad (24)$$

with c specifying a constant set to satisfy $||\mathbf{g}_{opt}||^2 = 1$. Also, the corresponding maximal ratio Q/J is $\lambda_{max}\{\mathbf{\Lambda}^{-1}\mathbf{\Psi}\}$.

Proof: We can formulate the given maximization problem as

$$\mathbf{g}_{opt} = \arg\max_{\mathbf{g}} \frac{\mathbf{g}\mathbf{\Psi}\mathbf{g}^H}{\mathbf{g}\mathbf{\Lambda}\mathbf{g}^H} \qquad (25)$$

subject to $||\mathbf{g}||^2 = 1$. Since $\mathbf{\Lambda}, \mathbf{\Psi}$ depends only on the window, not the filter, the proof follows directly by Rayleigh quotient result [18]. Therefore, the maximum power ratio is λ_{max}, the maximum eigenvalue of $\mathbf{\Lambda}^{-1}\mathbf{\Psi}$, and the optimal filter is proportional to the corresponding eigenvector. ∎

We note at this point that the optimization criterion used here essentially reduces to the signal to in-band distortion plus out-of-band leakage ratio (SDLR) criterion of [14], [15] in the special case where the window component is taken away and if a receiver-based on the $2N$-point FFT is used instead.

The elements of $\mathbf{\Lambda}_{ob}$, $\mathbf{\Lambda}_{ib}$, and $\mathbf{\Psi}$ are specified by the following three propositions (with proofs given in Appendices B and C).

Proposition 1. The element of $\mathbf{\Lambda}_{ob}$ at row m and column n is

$$\Lambda_{ob}(m,n)$$
$$= \sigma_X^2 \sum_{l=-N_1}^{N_1} \sum_{k=N_1+1}^{N-N_1-1} e^{-j2\pi(m-n)l/N} \mathbf{A}^*(n)_{k-l}\mathbf{A}(m)_{k-l} \qquad (26)$$

for $m, n \in [0, L_g - 1]$, where $\sigma_X^2 = \overline{|X_k|^2}$, and $\mathbf{A}(m)_{k-l}$ denotes the $(k-l)$-th element of the vector $\mathbf{A}(m)$. We utilized the cyclic property $\mathbf{A}(m)_{N+t} = \mathbf{A}(m)_t$ for the case $t < 0$.

Proposition 2. The element of $\mathbf{\Lambda}_{ib}$ at row m and column n is

$$\Lambda_{ib}(m,n)$$
$$= \sigma_X^2 \sum_{l=-N_1}^{N_1} \sum_{\substack{k=-N_1 \\ k\neq l}}^{N_1} e^{-j2\pi(m-n)l/N} \mathbf{A}^*(n)_{k-l}\mathbf{A}(m)_{k-l} \qquad (27)$$

for $m, n \in [0, L_g - 1]$.

Proposition 3. The element of $\mathbf{\Psi}$ at row m and column n is

$$\Psi(m,n) = \sigma_X^2 \mathbf{A}(m)_0 \mathbf{A}^*(n)_0 \alpha(m-n) \qquad (28)$$

for $m, n \in [0, L_g - 1]$, where

$$\alpha(k) = \begin{cases} \frac{\sin(\pi k N_{sb}/N)}{\sin(\pi k/N)}, & k \neq 0 \\ N_{sb}, & k = 0. \end{cases} \qquad (29)$$

With the elements of $\mathbf{\Lambda}_{ob}$, $\mathbf{\Lambda}_{ib}$ and $\mathbf{\Psi}$ completely specified by (26), (27) and (28), respectively, the optimum filter solution $\mathbf{g}_{opt}$ for a Nyquist window length N_{cp} can be obtained via eigen decomposition according to Lemma 2.

The observation that the product matrix $\mathbf{\Lambda}^{-1}\mathbf{\Psi}$ depends only on the window, not the filter, leads to a rather powerful statement:

Theorem 1. The window length corresponding to the maximal ratio Q/J is

$$N_{cp}^{opt} = \arg\max_{N_{cp}} \lambda_{max}\{\mathbf{\Lambda}^{-1}(N_{cp})\mathbf{\Psi}(N_{cp})\}, \qquad (30)$$
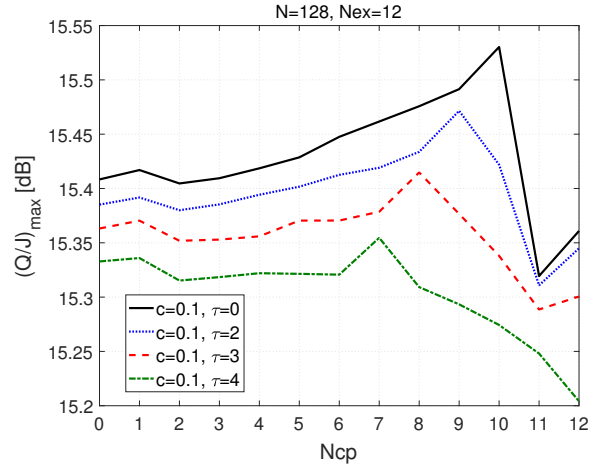

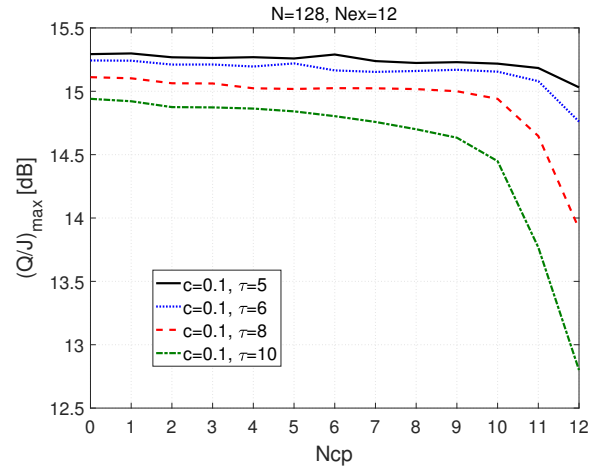Fig. 3. Maximum Q/J versus window length under the fixed excess frame length for c=0.1 and relatively small τ values.

Fig. 4. Maximum Q/J versus window length under the fixed excess frame length for c=0.1 and relatively large τ values.

(where $\mathbf{\Psi}$ and $\mathbf{\Lambda}$ are written as explicit functions of the window length N_{cp}) and the optimal filter $\mathbf{g}_{opt}$ yielding the maximal ratio is proportional to $\phi_{max}\{\mathbf{\Lambda}^{-1}(N_{cp}^{opt})\mathbf{\Psi}(N_{cp}^{opt})\}$.

Proof: The proof follows directly from Lemma 2. ∎

Once $\mathbf{\Psi}(N_{cp})$ and $\mathbf{\Lambda}(N_{cp})$ are found for all N_{cp}, the optimum window length and the corresponding filter can be specified according to Theorem 1.

For a fixed N_{ex}, what would be the best allocation between the Nyquist-window and the filter in combating the effect of STO and CFO? Figs. 3 and 4 show $(Q/J)_{max}$ versus the window length N_{cp} for $N_{ex} = 12$ and different values of τ. In Fig. 3 it is clear that there exists trade-off between N_{cp} and L_g under the constraint $N_{ex} = N_{cp} + L_g - 1$, although the difference between the largest and smallest $(Q/J)_{max}$ values is not that big for relatively small STO values. As clear in both figures, as τ becomes larger, filtering (and thus less windowing) tends to be more beneficial. Especially for fairly large STOs, setting N_{cp} greater than 10 (meaning using a filter with less than 3 taps) results in a substantial performance loss. Note that these results correspond to the cases where
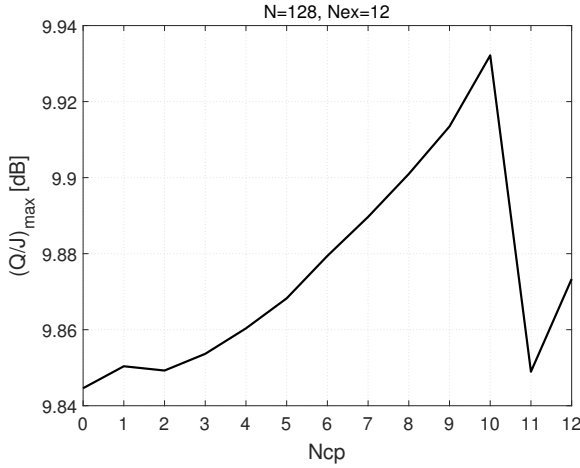
Fig. 5. Maximum averaged Q/J versus window length for uniformly distributed $c \in [-0.3, 0.3]$, $\tau \in [-N_{ex}, N_{ex}]$.

Fig. 6. Optimal filter for uniformly distributed $c \in [-0.3, 0.3]$, $\tau \in [-N_{ex}, N_{ex}]$.

the filter taps/window length are optimized for the given CFO and STO values. While these results provide insights into the performance limits of the best-designed filter/window, the assumed scenario of known CFO/STO values is not practical.

A more practical scenario would be to design the window/filter against distributions of CFO and STO. As in many previous studies [14], [15], [19], we assume uniform distributions of CFO/STO. Assuming $c \in [-c_{max}, c_{max}]$ and $\tau \in [-\tau_{max}, \tau_{max}]$, the $(Q/J)_{max}$ values and the optimum filters can be obtained by replacing every $\Lambda(m, n), \Psi(m, n)$ with

$$\overline{\Lambda}(m,n) = \frac{1}{2c_{max}(2\tau_{max}+1)} \sum_{\tau=-\tau_{max}}^{\tau_{max}} \int_{-c_{max}}^{c_{max}} \Lambda(m,n) \, dc$$

$$\overline{\Psi}(m,n) = \frac{1}{2c_{max}(2\tau_{max}+1)} \sum_{\tau=-\tau_{max}}^{\tau_{max}} \int_{-c_{max}}^{c_{max}} \Psi(m,n) \, dc$$

in $\mathbf{\Lambda}, \mathbf{\Psi}$. Fig. 5 shows $(Q/J)_{max}$ versus window length N_{cp} for uniformly distributed CFO/STO, where the ranges are assumed to be known: $c \in [-0.3, 0.3]$, $\tau \in [-N_{ex}, N_{ex}]$. Again $N_{ex} = 12$ is assumed. The optimal value is clearly $N_{cp} = 10$, and the corresponding filter responses in the time and frequency domains are shown in Fig. 6.

D. Minimizing Crossband Multiple Access Interference

Note that the above discussion reasonably reflects downlink communication where STOs/CFOs of subband of interest and the neighboring subbands have the similar range. For uplink, most of the previous investigations have considered controlling crossband multiple access interference (MAI) in frequency-division multiple access situation [2], [20]. There, the interference under consideration is the one that arises from the CFO/STO in the signals of the users in neighboring bands affecting the particular subband of interest. In such studies, the typical assumption is that the subband of interest is perfectly synchronized with no CFO/STO. We first consider minimizing MAI with a perfectly synchronized subband of interest, and
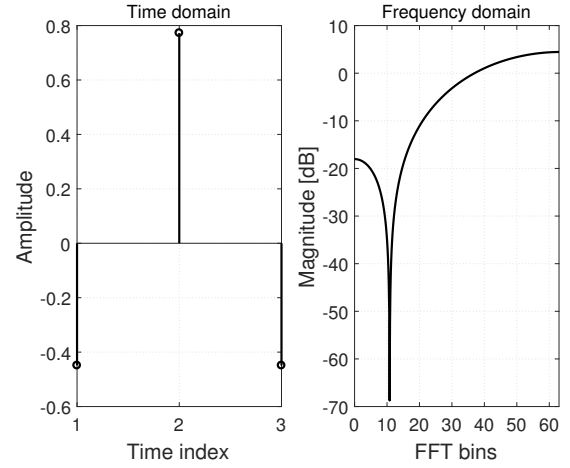
then also do analysis relaxing this assumption of the perfect main subband synchronization.

An equivalent way of measuring such MAI is to compute the power of interference terms that leak outside the subband of interest, with a possible guard band in place at the band edges. Our present analysis can easily be changed into MAI minimization. Assuming that there are N_{nl} null subcarriers on each edge of the subband, the MAI is the power of a truncated $\mathbf{e}_{ob}$:

$$\mathbf{e}_{ob} = \mathbf{g}\mathbf{E}_{ob}\mathbf{M}_{ob}$$

where

$$\mathbf{M}_{ob} = \text{diag}[\underbrace{0 \; 0 \; \cdots \; 0}_{1+N_1+N_{nl}} \; 1 \; 1 \cdots 1 \; 1 \; \underbrace{0 \; \cdots \; 0}_{N_1+N_{nl}}]$$

is a mask that suppresses the subband of interest plus the null subcarrier positions from the error vector.

We apply a normalization by a signal similar to the optimality criterion of Lemma 2. The objective function now is

$$\frac{Q}{J} = \frac{\mathbf{g}\mathbf{\Psi}\mathbf{g}^H}{\mathbf{g}\mathbf{\Lambda}_{ob}\mathbf{g}^H}$$

where $\mathbf{g}\mathbf{\Psi}\mathbf{g}^H$ is the undistorted signal power without any CFO/STO. Note that optimization using this objective function is akin to the use of the signal-to-leakage ratio (SLR) criterion of [14], [15]. Theorem 1 can be utilized in finding the minimum normalized MAI windowing/filtering solution using the following proposition.

Proposition 4. The element of $\mathbf{\Lambda}_{ob}$ at row m and column n is

$$\Lambda_{ob}(m,n)$$
$$= \sigma_X^2 \sum_{l=-N_1}^{N_1} \sum_{k=N_{nl}+N_1+1}^{N-N_{nl}-N_1-1} e^{-j2\pi(m-n)l/N} \mathbf{A}^*(n)_{k-l}\mathbf{A}(m)_{k-l}$$

(31)

for $m, n \in [0, L_g - 1]$.

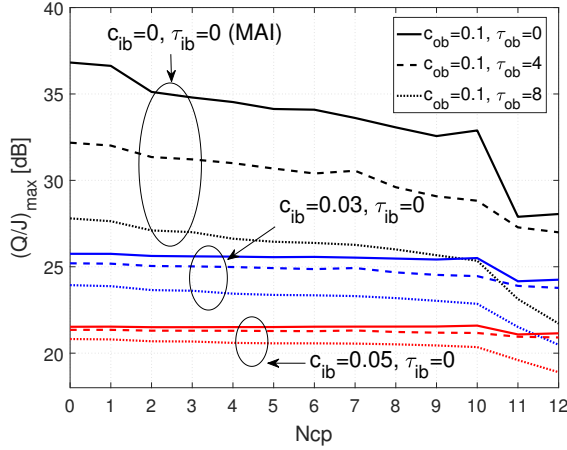*Proof:* Only considering the null subcarriers additionally, the proof follows directly from Proposition 1. ∎

Fig. 7. Maximum Q/J versus window length with one null subcarrier. In-band interference J_{ib} and signal power Q are calculated with fixed CFO/STO of $c_{ib} = 0$, $c_{ib} = 0.03$, $c_{ib} = 0.05$ while $\tau_{ib} = 0$. For out-of-band interference J_{ob}, CFO is fixed as $c_{ob} = 0.1$ with different STO values τ_{ob}.
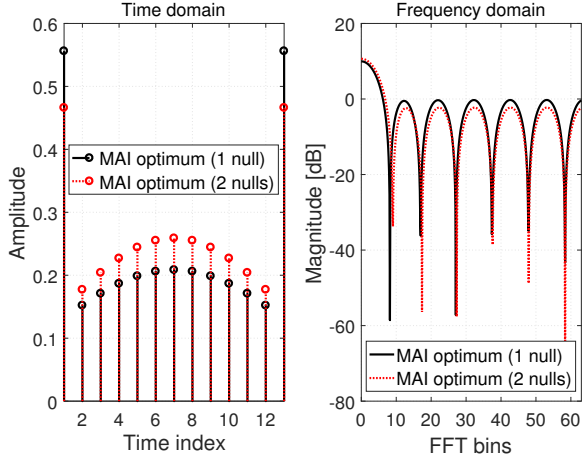

Fig. 8. Optimal MAI filter for uniformly distributed $c \in [-0.5, 0.5]$ and $\tau \in [-N_{ex}, N_{ex}]$.

Assuming a single null subcarrier, the best filter is obtained for a given window length. Fig. 7 shows maximum Q/J versus N_{cp} with different in-band and out-of-band CFO/STO values. Minimizing the normalized MAI coincides with the case of zero in-band CFO/STO: $c_{ib} = 0, \tau_{ib} = 0$. All out-of-band signals are distorted by CFO of c_{ob} and STO of τ_{ob}. The results show that UFMC (i.e, no windowing) is the best solution for minimizing MAI. For uniformly distributed $c \in [-0.5, 0.5]$ and $\tau \in [-N_{ex}, N_{ex}]$, the solution to the MAI problem becomes optimal when $N_{cp} = 0$ according to a plot similar to Fig. 7 (not shown in the paper due to the page limit). The optimal filter is shown in Fig. 8.

Fig. 7 also shows the cases for in-band CFO/STO of $(c_{ib}, \tau_{ib}) = (0.03, 0), (0.05, 0)$. By calculating in-band and out-of-band interferences J_{ib} and J_{ob} with different CFO/STO values, we simply maximize

$$\frac{Q}{J} = \frac{\mathbf{g}\mathbf{\Psi}(c_{ib}, \tau_{ib})\mathbf{g}^H}{\mathbf{g}[\mathbf{\Lambda}_{ob}(c_{ob}, \tau_{ob}) + \mathbf{\Lambda}_{ib}(c_{ib}, \tau_{ib})]\mathbf{g}^H}$$

where the dependence of $\mathbf{\Psi}$ and $\mathbf{\Lambda}$ on CFO/STO values are shown explicitly. The results indicate that increasing the window length up to 10 compromises very little performance, if any. This suggests that even in uplink, introducing window in the spectral shaping process is beneficial unless the synchronization in the subband of interest is ideal.

E. Minimizing Out of Band Power

In spectral aggregation, perhaps the most critical spectral shaping criterion is to reduce the OBP. The window/filter design that minimizes the interference power or the interference power scaled to the signal power does not necessarily minimize the OBP. Here we provide window/filter design guidelines oriented towards minimizing the OBP. We first define the OBP.

Under a raised-cosine Nyquist-window, let $W_\alpha(f)$ be the subcarrier spectrum corresponding to the window mix parameter α. The total signal power associated with all subcarriers in a given subband Ω_{SB} spread over all frequencies Ω is

$$P_S = \sum_{k \in \Omega_{SB}} \int_{f \in \Omega} |W_\alpha(f - k)G(f)|^2 df. \quad (32)$$

The signal power that leaks into some specific frequency band Ω_{OB} can also be expressed similarly:

$$P_{OB} = \sum_{k \in \Omega_{SB}} \int_{f \in \Omega_{OB}} |W_\alpha(f - k)G(f)|^2 df. \quad (33)$$

We wish to maximize the ratio P_S/P_{OB} for a given set $\{N_{ex}, \alpha, \Omega_{OB}\}$.

Lemma 3. The filter $\mathbf{g}$ of length $L_g = (1 - \alpha)N_{ex} + 1$ that maximizes the power ratio P_S/P_{OB} under the constraint $||\mathbf{g}||^2 = 1$ is given by

$$\mathbf{g}_{mobp} = c\, \phi_{max}\{\mathbf{V}^{-1}\mathbf{U}\} \quad (34)$$

where $\mathbf{U}$ and $\mathbf{V}$ are L_g by L_g Hermitian matrices with (m, n)-th elements given by

$$U_{m,n} = \sum_{k \in \Omega_{SB}} \int_{f \in \Omega} |W_\alpha(f - k)|^2 e^{-j2\pi f(m-n)/N} df$$

$$V_{m,n} = \sum_{k \in \Omega_{SB}} \int_{f \in \Omega_{OB}} |W_\alpha(f - k)|^2 e^{-j2\pi f(m-n)/N} df$$

with c specifying a constant to satisfy $||\mathbf{g}_{mobp}||^2 = 1$. Also, the corresponding maximal ratio P_S/P_{OB} is $\lambda_{max}\{\mathbf{V}^{-1}\mathbf{U}\}$.

Proof: See Appendix D. ∎

In designing the minimum OBP solution it is sometimes useful to allow a guard band between the subband of interest and the band over which the total signal leakage power is to be measured. This is because without any guard band or null subcarriers the OBP is often dominated by the significant portion of the main lobe and it is hard to achieve a meaningful level of sideband suppression. In the sequel we will assume, at the cost of a slightly reduced spectral efficiency, a single null subcarrier where the subband of interest borders the band of other users in spectral aggregation situation.
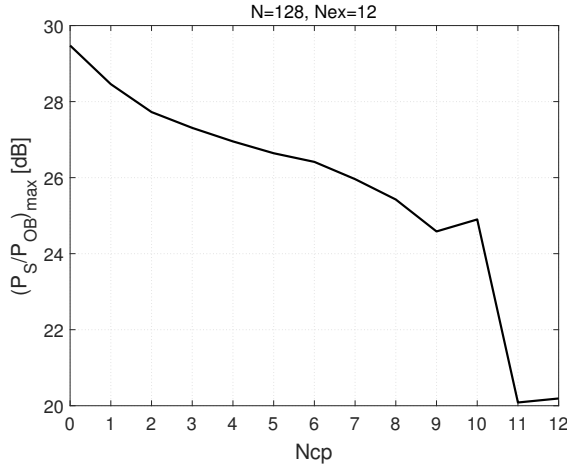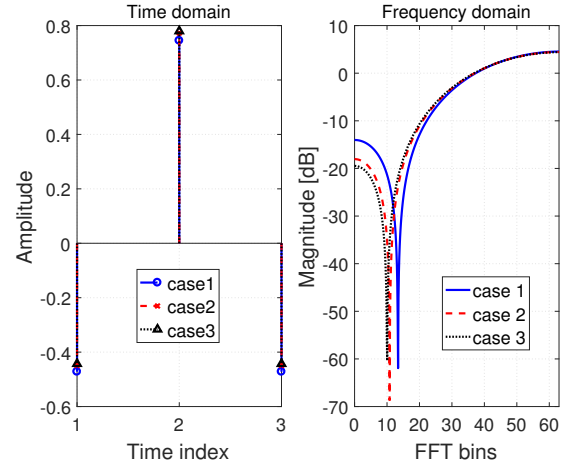
Fig. 9. Maximum P_S/P_{OB} versus window length under a constrained N_{ex}.

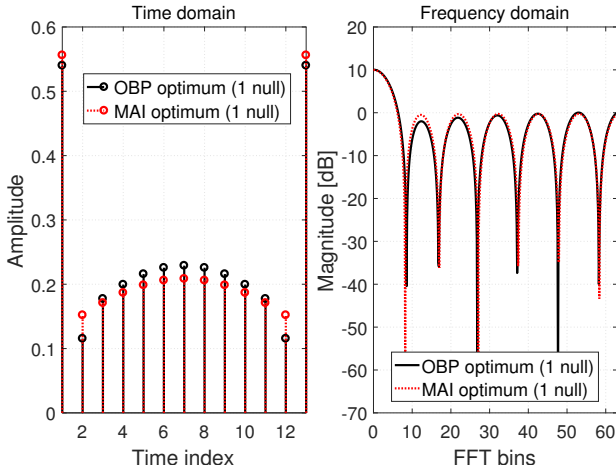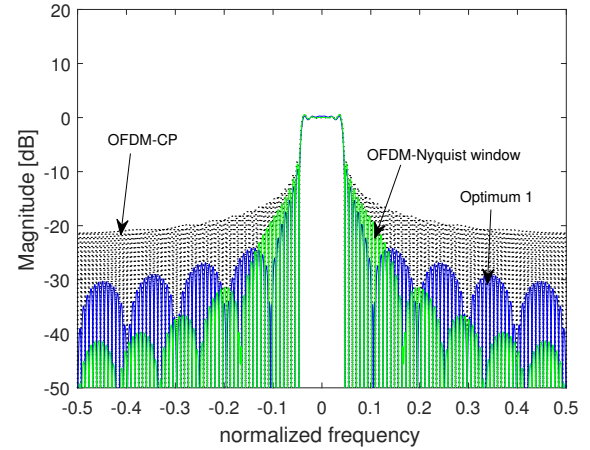Fig. 11. Optimum 1 filters for different cases.

Fig. 10. OBP optimum filter compared with MAI optimum filter assuming one null subcarrier. MAI filter is optimized for uniform range $c \in [-0.5, 0.5]$, $\tau \in [-N_{ex}, N_{ex}]$, $N_{ex} = 12$.

Fig. 12. Power spectrum for Optimum and full windowing. Optimum 1 is optimized for uniform distributions with $c \in [-0.1, 0.1]$, $\tau \in [-N_{ex}, N_{ex}]$.

Fig. 9 shows the optimal OBP versus window length assuming one null subcarrier. Similar to the MAI results, optimum is when $N_{cp} = 0$, which means UFMC is the best solution to reduce OBP. The filter taps of the optimal OBP solution are compared with the uniformly distributed MAI solution in Fig. 10 assuming a single null subcarrier. Two filters have similar ripples in the frequency domain.ompares the time domain impulse responses and the magnitude spectra of different filter/widow combinations under the fixed excess frame length constraint. Also shown are the Cheby-shev filter responses, which are also combined with windowing.

IV. NUMERICAL RESULTS AND PERFORMANCE COMPARISON

A. Window/Filter Properties

Table I shows the optimal N_{cp} length for different settings. FFT size $N = 128$ and excess frame length $N_{ex} = 12$ are assumed. The excess frame length N_{ex} is set to be less than 10% of the FFT size for low latency communication. Assuming an STO range of $\tau \in [-N_{ex}, N_{ex}]$ and three different asynchronous CFO ranges ± 0.1, ± 0.3, ± 0.5, all window/filter are optimized for uniform distributions. Let us denote the result of the first optimization criterion for downlink as Optimum 1 and the result of the second criterion focusing on reducing MAI, as Optimum 2. For Optimum 1, optimal N_{cp} is always 10 with filter length $L_g = 3$. The filters are shown in Fig 11. As CFO range gets bigger, the main lobe of the filter gets closer to the subband size and suppresses more interference leaking into the subbands near the main lobe. This result could be seen in Fig. 12, which compares the power spectrum of Optimum 1 for uniform distributions in the ranges $c \in [-0.1, 0.1]$ and $\tau \in [-N_{ex}, N_{ex}]$ with OFDM and Nyquist
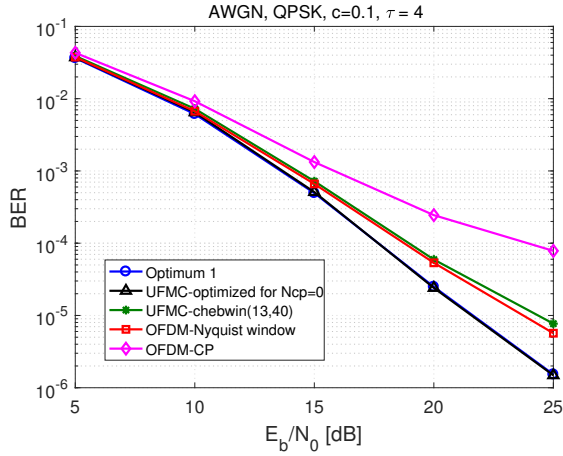
TABLE I
OPTIMAL N_{cp} LENGTH FOR $\tau \in [-N_{ex}, N_{ex}]$ AND THREE DIFFERENT CFO RANGES.

	CFO range		
	case 1 ± 0.1	case 2 ± 0.3	case 3 ± 0.5
Optimum 1	10	10	10
Optimum 2 (MAI)	0	0	0

Fig. 13. BER for $c = 0.1, \tau = 4$ in downlink. Window/filter are optimized for this specific case. AWGN channel.

Fig. 14. Sum-rate versus STO for fixed c=0.3 in downlink. All window/filter are optimized for $c \in [-0.3, 0.3]$, $\tau \in [-N_{ex}, N_{ex}]$. SNR = 20 dB.

windowing. For Optimum 2, we get $N_{cp} = 0$ for all ranges, which is just UFMC. This means filtering is more effective in suppressing the interference leaking into other subbands.

B. Downlink

The performance for the downlink scenario shows improvement by combining window/filter. This is noteworthy as the window component becomes stronger for a given excess length, the filtering requirement weakens, which leads to lower overall transmitter complexity. Thus, the downlink performance is improved while at the same time complexity is reduced by introducing windowing in the spectral shaping process. Assuming a single-data-symbol transmission, we now study bit error rate (BER) and sum-rate performances in the presence of CFO/STO-induced inter-carrier interference. All subbands suffer from CFO/STO, each having 11 subcarriers and no null subcarriers are assumed. We compare our results with UFMC using the Dolph-Chebyshev filter with side-lobe attenuation of 40 dB, OFDM using the raised-cosine Nyquist window of length 12, the same as our excess frame length, and OFDM with a cyclic prefix (CP) length of 12. We also compare our result with UFMC using the filter optimized for $N_{cp} = 0$ as done in [15] for maximizing the SDLR.

To gain insights, performance for specific $c = 0.1, \tau = 4$ case is compared first, where window/filter are optimized for this fixed condition. The filter length of Optimum 1 becomes 6 in this case. Fig. 13 shows BER performances assuming the AWGN channel. All window/filter methods provide performance advantage compared to the traditional OFDM with CP. With only 6 filter taps, Optimum 1 gives the same performance as the optimized UMFC with 13 filter taps. This indicates the advantage of introducing windowing, which leads to lower transmitter complexity. Both Optimum 1 and UFMC with an optimized filter exhibit performance gains over pure windowing and UFMC with a Dolph-Chebyshev filter.

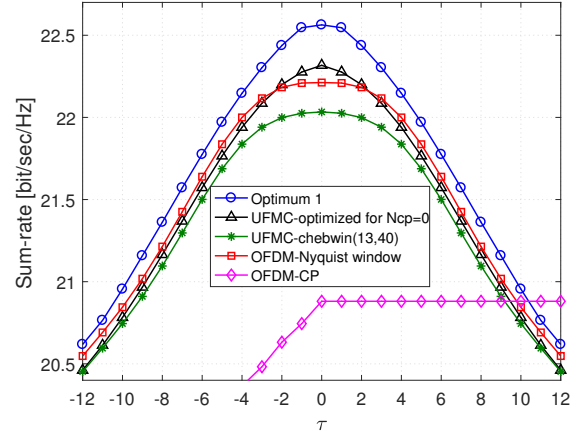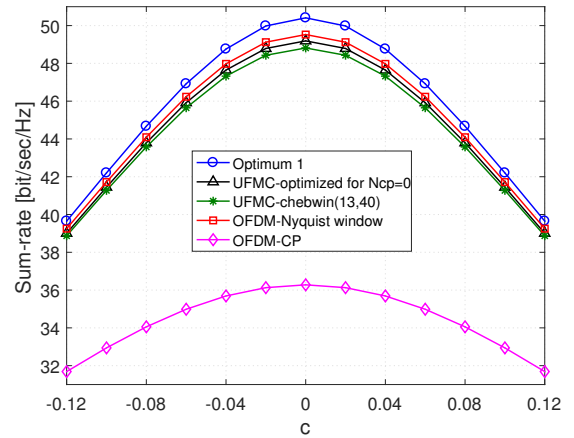We also compare the sum-rate performances. The sum-rate

Fig. 15. Sum-rate versus normalized CFO for fixed $\tau = -N_{ex}$ in downlink. Window/filter are optimized for $c \in [-0.3, 0.3]$, $\tau \in [-N_{ex}, N_{ex}]$. SNR = 20 dB.

is defined as

$$\sum_{k \in I_{sub}} \log_2(1 + \text{SINR}_k)$$

where I_{sub} is the subband of interest. The additive noise power is such that the total signal to total noise ratio of the subband is 20 dB. Again, in practical scenarios, we assume uniform distributions of CFO/STO. Fig. 14 shows sum-rate comparison for such a design over a range of STO values with CFO fixed at $c = 0.3$. For the results of Fig. 14, the window/filter are optimized assuming uniform distributions in $c \in [-0.3, 0.3]$, $\tau \in [-N_{ex}, N_{ex}]$. The performance curves are symmetric around $\tau = 0$ except the cyclic-prefixed OFDM. As long as $|\tau|$ does not exceed the CP length, CP-OFDM gives the same performance during the positive STO. For negative STOs, CP-OFDM exhibits performance losses like other waveforms. It is apparent that Optimum 1 with an ideal combination of window and filtering gives the best performance.

Sum-rates for the worst STO case have also been studied. Fig. 15 shows the sum-rate versus normalized CFO while STO is fixed as the worst case, $\tau = -N_{ex}$. As in the
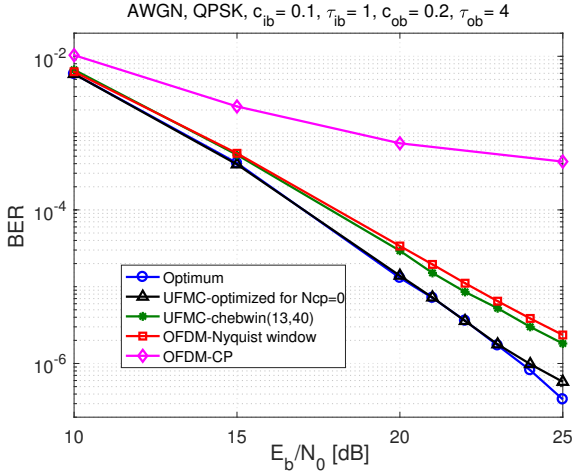
Fig. 16. BER for $c_{ib} = 0.1, \tau_{ib} = 1, c_{ob} = 0.2, \tau_{ob} = 4$ in uplink. Window/filter are optimized for this specific case. AWGN channel.

Fig. 18. Sum-rate versus out-of-band STO for fixed $c_{ib} = 0.1, \tau_{ib} = 6, c_{ob} = 0.2$ in uplink. SNR = 20 dB.
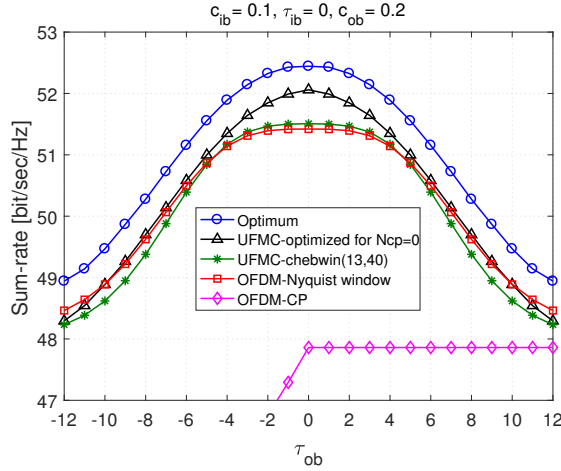

Fig. 17. Sum-rate versus out-of-band STO for fixed $c_{ib} = 0.1, \tau_{ib} = 0, c_{ob} = 0.2$ in uplink. SNR = 20 dB.

worst CFO situation, the sum-rate is improved by combining window/filter. Optimization is done assuming uniform distributions in $c \in [-0.3, 0.3]$, $\tau \in [-N_{ex}, N_{ex}]$.

C. Uplink

In uplink, if the subband of interest is perfectly synchronized, windowing does not give improvements for minimizing the MAI power. Windowing does not even give improvements for minimizing the OBP. So UFMC is preferred for uplink when perfect synchronization is possible. Performance of UFMC for this scenario was also studied in [15]. There, for each CFO/STO range, the filter that gives the best performance was different.

For imperfect main subband synchronization in uplink, Fig. 16 shows BER performances again assuming the AWGN channel. In-band distortion of $c_{ib} = 0.1, \tau_{ib} = 1$ and out-of-band interference of $c_{ib} = 0.2, \tau_{ob} = 4$ are assumed where window/filter are optimized for this specific case. Two null subcarriers are used between subbands with 10 users. The filter length of Optimum becomes 3 in this case. With only 3 filter
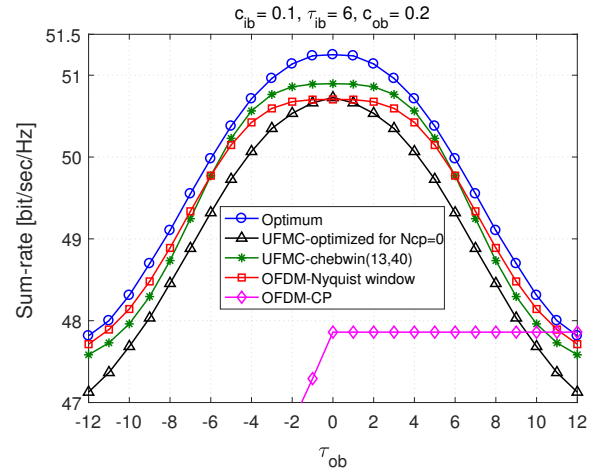
taps, Optimum gives better performance compared to UFMC with 13 filter taps, albeit by a small margin, while the gain is substantial compared to OFDM with CP.

Sum-rates are also studied with imperfect synchronization of subband of interest in uplink. The optimal N_{cp} is determined by how severe the out-of-band interference is and how precise synchronization can be. As out-of-band interference becomes dominant, filtering gives better results. Assuming perfect time synchronization and uniformly distributed $c_{ib} \in [-0.1, 0.1]$, consider two out-of-band interference cases. For uniformly distributed $c_{ob} \in [-0.5, 0.5]$, $\tau_{ob} \in [-N_{ex}, N_{ex}]$, $N_{cp} = 0$ is optimum while for $c_{ob} \in [-0.2, 0.2]$ and $\tau_{ob} \in [-N_{ex}, N_{ex}]$, $N_{cp} = 10$ gives optimum results. Using the window/filter optimized for $c_{ob} \in [-0.2, 0.2]$, $\tau_{ob} \in [-N_{ex}, N_{ex}]$, Figs. 17 and 18 show the sum-rate over a range of STOs in other subbands. For Fig. 17, perfect time synchronization is assumed while for Fig. 18, in-band STO of 5% is assumed. CFOs are fixed as $c_{ib} = 0.1, c_{ob} = 0.2$, and a single null subcarrier is used between subbands assuming 10 users. From Fig. 18, it can be seen that the UFMC-optimized for $N_{cp} = 0$ gives lower performance compared to others if the generated STO is not in the expected range. The results are consistent with the downlink analysis, confirming the advantage of the combined window/filter approach.

D. BERs in Multi-Path Channel

While the above analysis and performance evaluations are all based on the AWGN channel assumption, we also ran BER simulations of the various window/filter design options in the presence of multi-path interference. In Figs. 19 and 20, BER performances are summarized for the long term evolution (LTE) Extended Pedestrian A (EPA) channel with seven non-zero multi-paths [21] for downlink and uplink, respectively. All settings for Fig. 19 is the same as in Fig. 13 whereas that for Fig. 20 is consistent with that for Fig. 16. Compared to Figs. 13 and 16, the multi-path signal degrades all waveform options, but it is seen that the proposed optimum designs still remain competitive, offering desirable waveform solutions even in this multi-path channel.
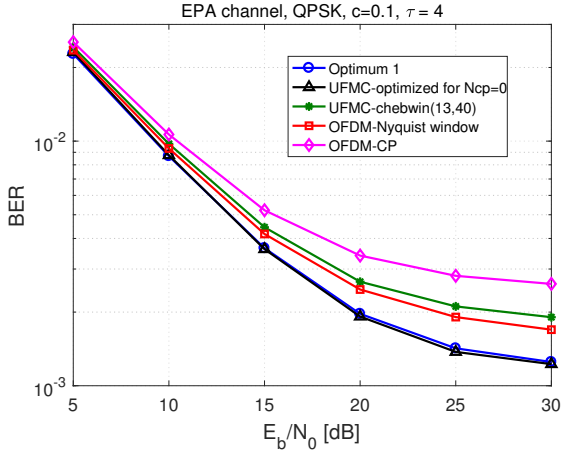
Fig. 19. BER for $c = 0.1, \tau = 4$ in downlink. Window/filter are optimized for this specific case. EPA channel.
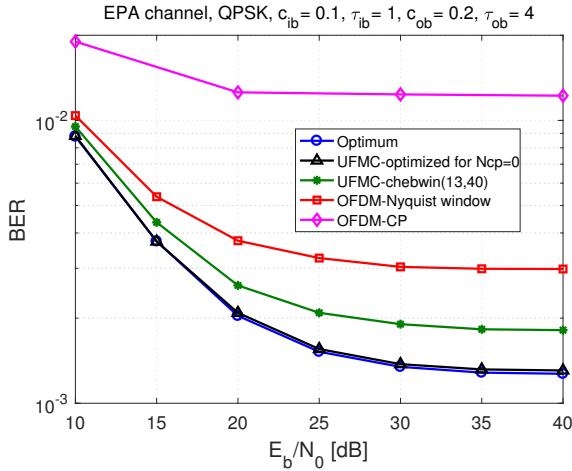

Fig. 20. BER for $c_{ib} = 0.1, \tau_{ib} = 1, c_{ob} = 0.2, \tau_{ob} = 4$ in uplink. Window/filter are optimized for this specific case. EPA channel.

V. Conclusions

Combined filtering and windowing has been suggested for controlling self-interference and spectral leakage of subband signals. An efficient receiver structure geared to the proposed combined spectrum control scheme has been devised. Under the fixed excess frame length constraint, this paper has provided an analytical tool based on the error signals and explored window-filter trade-off. For downlink, combining windowing and filtering is always beneficial as better performance is achieved at lower complexity, relative to pure filtering. For uplink, with perfect synchronization of the subband of interest, UFMC with no windowing component was the optimal solution for minimizing MAI power or OBP. With imperfect synchronization of the subband of interest, however, a combined window/filter combination can give improvements just as in downlink. This analytical tool can be used for even tighter excess frame length for 5G, where minimizing the transmission-reception latency is one of the key issues.

Appendix

A. Proof of Lemma 1:

The noiseless received signal vector $\bar{\mathbf{r}}$ is the sum of $\mathbf{z}(i)$ for all $i \in C_{sub}$, where $\mathbf{z}(i) = [z_0(i)\; z_1(i)\; \cdots\; z_{N+N_t-1}(i)]$. The signal $\mathbf{z}(i)$ in turn can be thought of as the weighted sum of delayed versions of the Nyquist-windowed data $\mathbf{y}(i)$, when the delays and weights reflect the combined filter/channel response $v_k(i)$. Of the L_v delayed components making up $\mathbf{z}(i)$, just focus on the l-th component for the time being. This component can be written as $[\mathbf{0}_l\; \mathbf{y}(i)\; \mathbf{0}_{N_t-N_{cp}-l}] \triangleq \mathbf{y}(i, l)$ with a prefixed string of l zeros corresponding to the delay and the tail zeros inserted simply to match the dimension. The tail-biting operation on this gives

$$\mathbf{y}(i, l)\mathbf{\Gamma}$$
$$= [\mathbf{x}(i)_{N-N_{cp}-l}^{N-N_{cp}-1}\quad \mathbf{x}(i)_{N-N_{cp}}^{N-1}\quad \mathbf{x}(i)_0^{N-N_{cp}-l-1}]$$
$$\circ [\mathbf{1}_l \qquad (\mathbf{w}_1^{N_{cp}} + \mathbf{w}_{N_{cp}}^1)\qquad \mathbf{1}_{N_{cp}+l}] \tag{35}$$

which simply reduces to $\mathbf{x}(i)^{\rightarrow(l+N_{cp})}$, a cyclically shifted original data frame, if $\mathbf{w}_1^{N_{cp}} + \mathbf{w}_{N_{cp}}^1 = \mathbf{1}$. Assuming this is satisfied, an additional DFT operation gives a phase-rotated frequency-domain symbol set:

$$\mathbf{y}(i, l)\mathbf{\Gamma}\mathbf{F} = \mathbf{P}(N_{cp}) \circ \mathbf{X}(i) \circ \mathbf{P}(l). \tag{36}$$

Summing over all L_v filter/channel paths for subband i gives

$$\sum_l v_l(i)\mathbf{y}(i, l)\mathbf{\Gamma}\mathbf{F} = \mathbf{P}(N_{cp}) \circ \mathbf{X}(i) \circ \sum_l v_l(i)\mathbf{P}(l)$$
$$= \mathbf{P}(N_{cp}) \circ \mathbf{X}(i) \circ \mathbf{V}(i)$$
$$= \mathbf{P}(N_{cp}) \circ [\mathbf{0}_{(i-1)N_{sb}}\quad \mathbf{V}(i)_i^{i+N_{sb}-1} \circ \mathbf{S}(i)\quad \mathbf{0}_{N-iN_{sb}}]$$

where the second equality holds since

$$\sum_l v_l(i)\mathbf{P}(l) = \mathbf{v}(i)\mathbf{F} = \mathbf{V}(i)$$

and the third equality is due to $\mathbf{X}(i)$ being filled with zeros except for the i-th segment occupied by $\mathbf{S}(i)$. Including the signals from all subbands fills all remaining segments with the weighted data symbols; specifically, we obtain

$$\bar{\mathbf{r}}\mathbf{\Gamma}\mathbf{F} = \sum_{i,l} v_l(i)\mathbf{y}(i, l)\mathbf{\Gamma}\mathbf{F} \tag{37}$$

leading to (1).

B. Proofs of Propositions 1 and 2:

From $\mathbf{\Lambda}_{ob} = \overline{\mathbf{E}_{ob}\mathbf{M}_{ob}\mathbf{M}_{ob}^H\mathbf{E}_{ob}^H}$, we start by writing

$$\Lambda_{ob}(m, n) = \overline{\boldsymbol{\epsilon}_{ob}(m)\mathbf{M}_{ob}\mathbf{M}_{ob}^H\boldsymbol{\epsilon}_{ob}(n)^H}$$
$$= [\mathrm{tr}\{\mathbf{M}_{ob}^H\overline{\boldsymbol{\epsilon}_{ob}^H(m)\boldsymbol{\epsilon}_{ob}(n)}\mathbf{M}_{ob}\}]^*$$
$$= \sigma_X^2\,[\mathrm{tr}\{\mathbf{M}_{ob}\mathbf{A}_m^H\mathbf{P}_{m-\tau+N_{cp}}^H\mathbf{M}\mathbf{P}_{n-\tau+N_{cp}}\mathbf{A}_n\}]^*$$
$$= \sigma_X^2\,[\mathrm{tr}\{\mathbf{M}_{ob}\mathbf{A}_m^H\mathbf{P}_{m-n}^H\mathbf{M}\mathbf{A}_n\}]^*$$
$$= \sigma_X^2\,[\mathrm{tr}\{\mathbf{A}_n\mathbf{M}_{ob}\mathbf{A}_m^H\mathbf{P}_{m-n}^H\mathbf{M}\}]^*$$

where $\mathbf{M} = \mathrm{diag}[\mathbf{1}_{N_1+1}\; \mathbf{0}_{N-N_{sb}}\; \mathbf{1}_{N_1}]$, a masking matrix that arises since $\overline{\mathbf{X}^H\mathbf{X}} = \sigma_X^2 \times \mathrm{diag}[\mathbf{1}_{N_1+1}\; \mathbf{0}_{N-N_{sb}}\; \mathbf{1}_{N_1}]$ under the

assumption that the independent frequency-domain symbols occupy only the subband centered around the zero frequency. The last equality is due to the cyclic property of the trace.

The (l,k)-th element of $\mathbf{A}_n\mathbf{M}_{ob}$ is given by $\mathbf{A}(n)_{k-l}$ for $k \in [N_1+1, N-N_1-1]$ while being zero for all other values of k. The (l,k)-th element of $\mathbf{A}^*(m)$ is given by $\mathbf{A}^*(m)_{k-l}$. So the (l,l)-th element of $\mathbf{A}_n\mathbf{M}_{ob}\mathbf{A}_m^H\mathbf{P}_{m-n}^H$ can be written as

$$\sum_{k=N_1+1}^{N-N_1-1} e^{j2\pi(m-n)l/N}\mathbf{A}(n)_{k-l}\mathbf{A}^*(m)_{k-l}. \tag{38}$$

By taking a sum over those positions for which $\mathbf{M}$ is non-zero, i.e., $l \in [0, N_1] \cup [N-N_1, N-1]$, and taking the conjugate, we subsequently get

$$\sum_{l=-N_1}^{N_1}\sum_{k=N_1+1}^{N-N_1-1} e^{-j2\pi(m-n)l/N}\mathbf{A}^*(n)_{k-l}\mathbf{A}(m)_{k-l} \tag{39}$$

which leads to (26).

The proof of Proposition 2 is similar to the proof for Proposition 1.

C. Proof of Proposition 3:

From (23) we write

$$\Psi(m,n)$$
$$= \sigma_X^2 \sum_{l=-N_1}^{N_1} \mathbf{A}(m)_0\mathbf{P}(m+N_{cp})_l\mathbf{P}^*(n+N_{cp})_l\mathbf{A}^*(n)_0$$
$$= \sigma_X^2 \sum_{l=-N_1}^{N_1} \mathbf{A}(m)_0\mathbf{P}(m-n)_l\mathbf{A}^*(n)_0$$
$$= \sigma_X^2 \mathbf{A}(m)_0\mathbf{A}^*(n)_0 \sum_{l=-N_1}^{N_1} e^{-j2\pi(m-n)l/N}$$

which leads to (28).

D. Proof of Lemma 3:

Given the filter $\mathbf{g} = [g_0 \ g_1 \ ... \ g_{L_g-1}]$, we write

$$\mathbf{g}\mathbf{U}\mathbf{g}^H = \sum_{m=0}^{L_g-1}\sum_{n=0}^{L_g-1} U_{m,n} \ g_m g_n$$
$$= \sum_{k\in\Omega_{SB}} \int_{f\in\Omega} |W_\alpha(f-k)|^2 \sum_{m=0}^{L_g-1}\sum_{n=0}^{L_g-1} g_m g_n e^{-j2\pi f(m-n)/N} df$$
$$= \sum_{k\in\Omega_{SB}} \int_{f\in\Omega} |W_\alpha(f-k)G(f)|^2 df$$

which is P_S. Similarly, it is easy to show

$$\mathbf{g}\mathbf{V}\mathbf{g}^H = \sum_{k\in\Omega_{SB}} \int_{f\in\Omega_{OB}} |W_\alpha(f-k)G(f)|^2 df = P_{OB}.$$

We can now formulate the maximization problem as

$$\mathbf{g}_{mobp} = \arg\max_{\mathbf{g}} \frac{\mathbf{g}\mathbf{U}\mathbf{g}^H}{\mathbf{g}\mathbf{V}\mathbf{g}^H}$$

subject to $||\mathbf{g}||^2 = 1$. From the proof of Lemma 2, we can obtain the solution (34).

REFERENCES

[1] M. Simsek, A. Aijaz, M. Dohler, J. Sachs, and G. Fettweis, "5G-Enabled Tactile Internet" *IEEE Journal on Selected Areas in Communications*, vol. 34, no. 3, pp. 460-473, 2016.

[2] G. Wunder, P. Jung, M. Kasparick, T. Wild, F. Schaich, Y. Chen, S. Ten Brink, I. Gaspar, N. Michailow, A. Festag et al., "5GNOW: Non-orthogonal, asynchronous waveforms for future mobile applications," *IEEE Communications Magazine*, vol. 52, no. 2, pp. 97-105, 2014.

[3] J. G. Andrews, S. Buzzi, W. Choi, S. V. Hanly, A. Lozano, A. C. K. Soong, and J. C. Zhang, "What will 5G be?," *IEEE Journal on Selected Areas in Communications*, vol. 32, no. 6, pp. 1065-1082, Jun. 2014.

[4] F. E. H. Germany and A. C. France, "5G waveform candidate selection."

[5] P. Tan and N. C. Beaulieu, "Reduced ICI in OFDM systems using the better than raised-cosine pulse," *IEEE Communications Letters*, vol. 8, no. 3, pp. 135-137, 2004.

[6] P. Tan and N. C. Beaulieu, "Analysis of the effects of Nyquist pulse shaping on the performance of OFDM systems with carrier frequency offset" *European Transactions on Telecommunications*, vol. 20, no. 1, pp. 9-22, 2009.

[7] J. Di and C. Li, "Improved Nyquist windows for reduction of ICI in OFDM systems", *IEEE 4th International Symposium on MAPE*, pp. 438-441, 2011.

[8] S. H. Müller-Weinfurtner, "Optimum Nyquist windowing in OFDM receivers," *IEEE Transactions on Communications*, vol. 49, no. 3, pp. 417-420, 2001.

[9] B. Farhang-Boroujeny, "OFDM versus filter bank multicarrier," *IEEE Signal Processing Magazine*, vol. 28, no. 3, pp. 92-112, 2011.

[10] M. Bellanger, D. Le Ruyet, D. Roviras, M. Terre, J. Nossek, L. Baltar, Q. Bai, D. Waldhauser, M. Renfors, T. Ihalainen et al., "FBMC physical layer: A primer," *PHYDYAS*, 2010.

[11] G. Fettweis, M. Krondorf, and S. Bittner, "GFDM–Generalized Frequency Division Multiplexing," *IEEE VTC Spring*, pp. 1-4, 2009.

[12] N. Michailow, M. Matthe, I. S. Gaspar, A. N. Caldevilla, L. L. Mendes, A. Festag, and G. Fettweis., "Generalized frequency division multiplexing for 5th generation cellular networks," *IEEE Transactions on Communications*, vol. 62, no. 9, pp. 3045-3061, 2014.

[13] V. Vakilian, T. Wild, F. Schaich, S. ten Brink, and J.-F. Frigon, "Universal-filtered multi-carrier technique for wireless systems beyond LTE," in *Proc. IEEE Globecom Workshop*, pp. 223-228, 2013.

[14] X. Wang, T. Wild, F. Schaich, and A. F. Dos Santos, "Universal filtered multi-carrier with leakage-based filter optimization," *European Wireless,*, pp. 1-5, 2014.

[15] X. Wang, T. Wild, F. Schaich, "Filter optimization for carrier frequency and timing offsets in universal filtered multi-carrier system", *IEEE VTC Spring*, pp. 1-6, 2015.

[16] F. Schaich, T. Wild, and Y. Chen, "Waveform contenders for 5G suitability for short packet and low latency transmissions," *IEEE VTC Spring*, pp. 1-5. 2014.

[17] K. Lee, M. Kang, E.-R. Jeong, D.-J. Park, and Y. H. Lee, "Use of training subcarriers for synchronization in low latency uplink communication with GFDM," *IEEE Signal Processing Advances in Wireless Communications (SPAWC)*, pp. 1-6 2016.

[18] G. Golub and C. V. Loan, *Matrix Computations*, Johns Hopkins Univ. Press, vol. 3, 2012

[19] B. Lu, X. Wang, "Bayesian blind turbo receiver for coded OFDM systems with frequency offset and frequency-selective fading" *IEEE Journal on Selected Areas in Communications*, vol. 19, no. 12, pp. 2516-2527, 2001.

[20] A. Aminjavaheri, A. Farhang, A. RezazadehReyhani, and B. Farhang-Boroujeny, "Impact of timing and frequency offsets on multicarrier waveform candidates for 5G," *IEEE Signal Processing and Signal Processing Education Workshop (SP/SPE)*, pp. 178-183, 2015.

[21] 3GPP TS 36.101, "User Equipment (UE) radio transmission and reception," v.8.5.1, 2008.

Dong-Jun Han received B.S. degrees in Mathematics and Electrical Engineering from Korea Advanced Institute of Science and Technology (KAIST), Daejeon, Korea, in 2016. He is currently pursuing the M.S. degree in KAIST. His research interests include 5G Communications and machine learning.

Jaekyun Moon received the Ph.D degree in electrical and computer engineering at Carnegie Mellon University, Pittsburgh, Pa, USA. He is currently a Professor of electrical enegineering at KAIST. From 1990 through early 2009, he was with the faculty of the Department of Electrical and Computer Engineering at the University of Minnesota, Twin Cities. He consulted as Chief Scientist for DSPG, Inc. from 2004 to 2007. He also worked as Chief Technology Officier at Link-A-Media Devices Corporation. His research interests are in the area of channel characterization, signal processing and coding for data storage and digital communication. Prof. Moon received the McKnight Land-Grant Professorship from the University of Minnesota. He received the IBM Faculty Development Awards as well as the IBM Partnership Awards. He was awarded the National Storage Industry Consortium (NSIC) Technical Achievement Award for the invention of the maximum transition run (MTR) code, a widely used error-control/modulation code in commercial storage systems. He served as Program Chair for the 1997 IEEE Magnetic Recording Conference. He is also Past Chair of the Signal Processing for Storage Technical Committee of the IEEE Communications Society, In 2001, he cofounded Bermai, Inc., a fabless semiconductor start-up, and served as founding President and CTO. He served as a guest editor for the 2001 IEEE JSAC issue on Signal Processing for High Density Recording. He also served as an Editor for IEEE TRANSACTIONS ON MAGNETICS in the area of signal processing and coding for 2001-2006. He is an IEEE Fellow.
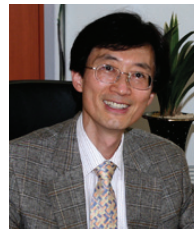
Dongjae Kim received the B.S. and M.S. degrees in electrical engineering from Korea Advanced Institute of Science and Technology (KAIST), Daejeon, Korea, in 2011 and 2013, respectively. He is currently pursuing the Ph.D degree in KAIST. His research interests include Faster-than-Nyquist (FTN) signaling and waveform design.

Sae-Young Chung received the B.S. and M.S. degrees in electrical engineering from Seoul National University, Seoul, South Korea, in 1990 and 1992, respectively and the Ph.D. degree in electrical engineering and computer science from the Massachusetts Institute of Technology, Cambridge, MA, USA, in 2000. From September 2000 to December 2004, he was with Airvana, Inc., Chelmsford, MA, USA. Since January 2005, he has been with the Department of Electrical Engineering, KAIST, Daejeon, South Korea, where he is currently a Professor. He served as an Associate Editor for the IEEE Transactions on Communications from 2009 to 2013. He has been serving as an Associate Editor for Shannon Theory for the IEEE Transactions on Information Theory since 2014. He served as the Technical Program Co-Chair of the 2014 IEEE International Symposium on Information Theory and the 2015 IEEE Information Theory Workshop. His research interests include information theory and machine learning.

Yong H. Lee received the B. S. and M. S. Degrees in Electrical Engineering from Seoul National University, Seoul, Korea, in 1978 and 1980, respectively, and the Ph.D. degree in Electrical Engineering from the University of Pennsylvania, Philadelphia, U. S. A., in 1984.

From 1984 to 1988, he was an Assistant Professor with the Department of Electrical and Computer Engineering, State University of New York, Buffalo. Since 1989, he has been with the Department of Electrical Engineering, Korea Advanced Institute of Science and Technology (KAIST), where he is currently a Professor. He was the Provost from 2011 to 2013, the Dean of Engineering from 2005 to 2011 and the Head of Electrical Engineering from 2004 to 2005, all in KAIST. His research activities are in the area of communication signal processing, which includes interference management, resource allocation, synchronization, detection and estimation for multiple-input multiple-output, wireless communication systems including line-of-sight communications and millimeter wave communication systems.